Journal of Drug Delivery Science and Technology 59 (2020) 101911

Contents lists available at ScienceDirect

Journal of Drug Delivery Science and Technology

journal homepage: www.elsevier.com/locate/jddst

Research paper

Green synthesis of zinc oxide nanoparticles by Neem extract as multi-facet therapeutic agents

Muhammad Farhan Sohail [a,b,c,*], Mubashar Rehman [b], Syed Zajif Hussain [c], Zil-e Huma [c], Gul Shahnaz [b], Omer Salman Qureshi [d], Qandeel Khalid [e], Shaper Mirza [f], Irshad Hussain [b], Thomas J. Webster [g,**]

[a] Riphah Institute of Pharmaceutical Sciences (RIPS), Riphah International University, Lahore Campus, Lahore, Pakistan
[b] Department of Pharmacy, Faculty of Biological Sciences, Quaid-i-Azam University, Islamabad, 45320, Pakistan
[c] Department of Chemistry and Chemical Engineering, SBA School of Science and Engineering (SBA-SSE), Lahore University of Management Sciences (LUMS), Lahore, 54792, Pakistan
[d] Department of Pharmacy, Forman Christian College University, Lahore, Pakistan
[e] Department of Pharmacy, The University of Faisalabad, Faisalabad, 38000, Pakistan
[f] Department of Biology, SBA School of Science and Engineering (SBA-SSE), Lahore University of Management Sciences (LUMS), Lahore, 54792, Pakistan
[g] Department of Chemical Engineering, Northeastern University, Boston, MA, 02115, USA

ARTICLE INFO

Keywords:
ZnO nanoparticles
Antibiotic-resistant bacteria
Antioxidant assay
Levofloxacin
Azadirachta indica and Neem extract

ABSTRACT

This study was designed to develop green synthesized zinc oxide nanoparticles (ZnO-NPs) as potential nano-antibiotics against drug resistant microbes along with multifarious biomedical applications. The developed ZnO-NPs with an average size of 19.57 ± 1.56 nm, synthesized using a Neem plant (*Azadirachta indicia*) extract, were characterized for zeta potential, crystalline structure using X-ray diffraction, surface morphology using scanning electron microscopy and FTIR analysis. The ZnO-NPs demonstrated a far superior antioxidant and enzyme inhibition activity with a significantly lower IC_{50} value as compared to a standard reference. Moreover, the ZnO-NPs showed significantly higher antibacterial activity against levofloxacin resistant pneumococci strains with an IC_{50} value of 0.014 μM compared to 2.048 mM for that of levofloxacin. An *in vivo* acute toxicity study in mice showed slight changes in liver functional tests, especially renal functional tests, compared to that of the control group. Complete blood analysis showed no significant changes. Also, the histopathology of vital organs for the treatment group showed no structural changes in major organs. Overall, the results suggested that the present green synthesized Neem based ZnO-NPs could be developed as a therapeutic agent with antioxidant, enzyme inhibition and strong antibacterial potential against antibiotic-resistant bacteria that can be safely administered.

1. Introduction

Several chemical and biological methods have been reported for ZnO nanoparticle (NPs) synthesis. However, 'green synthesis' is one of the most eco-friendly methods, where materials from plants are utilized for the stable synthesis of metal nanoparticles on a large scale [1,2]. The green process offers several advantages, which include simplicity of the procedure, a one-step process, cost-effectiveness, and reproducibility [3]. Although microorganisms can also be used to produce nano-particles, the rate of formation is slow compared to rates involving plant-mediated synthesis [4,5]. Extracts from different plants (like coffee, tea, fruits, vegetable, simple amino acids, and starch) can be used for capping or as reducing agents to produce stable metal or metal oxide nanoparticles. ZnO-NPs prepared using green approaches are believed to be non-toxic and bio-compatible which are highly desirable especially for biomedical applications, such as drug carriers, cosmetics, and fillings in medical materials [6]. Silver, gold, copper, zinc, carbon, and iron nanoparticles have successfully been fabricated *via* green synthesis for various applications, often showing better properties than those made through conventional synthetic routes [7,8].

* Corresponding author. Riphah Institute of Pharmaceutical Sciences (RIPS), Riphah International University, Lahore Campus, Lahore, Pakistan.
** Corresponding author. Department of Chemical Engineering, Northeastern University, Boston, MA, 02115, USA.
E-mail addresses: farhan.sohail@riphah.edu.pk, farmacist.pk@gmail.com (M.F. Sohail), th.webster@northeastern.edu (T.J. Webster).

https://doi.org/10.1016/j.jddst.2020.101911
Received 16 April 2020; Received in revised form 15 June 2020; Accepted 30 June 2020
Available online 16 July 2020

ZnO nanoparticles (ZnO-NPs) are becoming increasingly important in the health industry for the following reasons: unique antimicrobial and wound healing ability, UV filtration capacity, high catalytic and photochemical activities [9]. The antimicrobial activities of ZnO-NPs depend on their particle size, concentration, morphology and specific surface area. Antimicrobial efficacy has been reported to increase with decreasing particle size from bulk ZnO to smaller white ZnO-NPs. The antibacterial activity of ZnO nanoparticles results from a large concentration of H_2O_2 produced from the surface of the nanoparticles [10,11]. However, the conventional precipitation of ZnO-NPs usually involves zinc nitrate which has a moderate health warning and is a strong oxidizer, thus, avoiding the use of zinc nitrate would be beneficial for ZnO-NP production.

The biosynthesis of ZnO-NPs by plants such as *Aloe barbadensis*, *Sargassum muticum Parthenium hysterophorus, Aspergillus niger, Abrus precatorius*, etc. has been reported with antibacterial and antifungal activities [12,13]. *Azadirachta indicia*, also known as Neem, Nim tree, and Indian Lilac, is an indigenous tree in the mahogany family *Meliaceae*. It is one of the two species in the genus *Azadirachta* and is native to India, Nepal, Pakistan, Bangladesh, and Sri Lanka. Medicines made from Neem trees have been used in India for over two millennia. Neem products have been an important part of the Ayurvedic prescription for its activity against microbes and parasites and it has been used in cosmetics, such as products for hair care. Additionally, Neem derived products have also been used to improve liver function, detoxify the blood, and balance blood sugar levels. Neem leaves have also been used to treat skin diseases like eczema and psoriasis [14].

The potential use of these nanoparticles is vast and ranges from antioxidants to antimicrobials. The antioxidant property of these nanoparticles could be explored to treat excessive reactive oxygen species in diseases such as cancer and metabolic syndrome, and similarly, the enzyme inhibition activity of ZnO-NPs can inhibit key enzymes involved in numerous metabolic diseases [15]. Moreover, the antibacterial potential against various bacterial strains, in particular, drug-resistant bacterial strains, can be of significant value, especially in the current era when the world is faced with an epidemic of multi-drug resistant microorganisms [16].

Herein, we report a facile green method for the synthesis of ZnO-NPs using the Neem (*Azadirachta indicia*) extract as a reducing and stabilizing agent. These ZnO-NPs were characterized for various physiochemical parameters including particle size, zeta potential, surface morphology, functional moieties, and lattice parameters. Nanoparticles were further evaluated for their antioxidant, antimicrobial and enzyme inhibition activities. Finally, unlike most studies, we also measured their *in vivo* toxicity to establish a biocompatibility profile for the ZnO-NPs.

2. Materials and methods

2.1. Materials

$ZnSO_4{\cdot}7H_2O$, butylated hydroxytoluene, sulphuric acid, sodium phosphate, ammonium molybdate, acetate buffer, diphenyl picryl hydrazine, Follin & ceucalteu's phenol reagent, p-nitro phenyl glucose pyranose, sodium hydrogen phosphate, Tripyridyltriazine (TPTZ), gallic acid, DMSO and acarbose were all purchased from Sigma Aldrich, USA. NaOH, HCl, ethyl acetate, methanol, and acetone were purchased from Merck, Germany. All other solvents, solutions and chemicals used were of research grade.

2.2. Methods

2.2.1. Extraction of the Neem extract

ZnO-NPs were prepared using an aqueous extract of *Azadirachta indica* following a method reported earlier with slight modification [17]. The extract was isolated from the leaves of *Azadirachta indica* under ambient conditions. In a typical extraction, an excess of an aqueous NaOH solution (pH-11) was poured into the crushed, dried and powdered plant material. The mixture was heated on a water bath with continuous stirring for 1 h and then left to stir for 12 h. The alkaline extract was filtered, acidified with 10 mL of an aqueous HCl solution (pH = 1), and was allowed to stand for precipitation. The precipitate (containing a natural surfactant and byproducts) was separated by filtration. The residue was washed with distilled water and pre-extracted with ethyl acetate by refluxing for about 5–6 h. The extract was distilled off and the residue was extracted with acetone. The acetone extract was allowed to stand overnight. The precipitate obtained was a mixture of natural surfactant which was finally separated and dried.

2.2.2. Synthesis of ZnO-NPs

In a reaction flask, 22 mL of an aqueous solution containing $ZnSO_4{\cdot}7H_2O$ (1 M) and a natural surfactant (4 mL) was mixed with 12 mL of an aqueous solution of NaOH (4 M). The resulting mixture in the flask was stirred vigorously under room temperature and then the respective reaction flask was exposed to reaction conditions by placing them in a microwave oven (1 min). The ZnO-NP precipitates produced were filtered, washed with distilled water and then dried at room temperature [18].

2.2.3. DLS measurements and particle morphology

The hydrodynamic diameter and surface zeta potential of ZnO-NPs were measured using a Zetasizer (Malvern, NanoZSP, UK). The surface morphology of all the formulations was studied by a scanning electron microscope (SEM) (FEI, Nova NanoSEM 450, USA) operating at 17.5 kV. Samples for SEM were prepared by slowly evaporating a dilute drop of a ZnO-NPs suspension on a carbon-coated copper grid blotted with a drop of a 1% ammonium molybdate solution [19].

2.2.4. FTIR and XRD analysis

Fourier Transformed Infrared (FTIR) spectroscopy and X-ray diffraction analysis were used to characterize the ZnO NPs. The functional moieties from the pure plant extract responsible to stabilize these particles were identified using FTIR (Bruker, alpha-P) spectroscopy [20]. The XRD patterns of the particles were monitored using a powder X-ray diffractometer (Bruker, D2 Phaser) operating at 30 kV, 10 mA and using Cu $K\alpha 1$ radiation having $\lambda = 1.5406$ Å and adjusting the angle in the range $20 - 70^{\circ}$ with a step size of 0.0505°. The average size of the ZnO NPs was also calculated by using the Debye-Scherrer formula [21].

$$D = K\lambda/\beta \cos\theta$$

Where D is the average particle size in nm, λ is the wavelength of the X-ray (0.15406 nm), β is full width at half maximum (FWHM) of the diffraction peak, K is the Scherrer constant with the value of 0.9–1 and θ is the Bragg angle ($\theta = 2\theta/2$).

2.2.5. Antioxidant activity

The antioxidant potential of the ZnO-NPs was evaluated using three different techniques as described below.

2.2.5.1. 1,1-Diphenyl-2-picrylhydrazyl (DPPH) radical scavenging activity. The DPPH radical scavenging activities of various fractions of the plant were examined by comparison with that of a known antioxidant, butylated hydroxytoluene (BHT) [22]. Briefly, different concentrations of the samples (1000 μg/mL, 500 μg/mL, and 250 μg/mL) were mixed with 3 mL of a methanolic solution of DPPH (0.1 mM). The mixture was shaken vigorously and allowed to stand at room temperature for 1 h. After that, the absorbance was measured at 517 nm against methanol as a blank using a microtitration plate reader (Synergy HT, Biotech, USA). A lower absorbance from the spectrophotometer indicated higher free radical scavenging activity. The percent of DPPH discoloration of the samples was calculated according to the following formula:

$$\text{Antiradical activity} = \frac{Abs\ (control) - Abs\ (Sample)}{Abs\ (control)}\ X\ 100$$

2.2.5.2. Phosphomolybdenum complex method. Briefly, 500 μg/mL of each sample was mixed with 4 mL of a reagent solution (0.6 M sulphuric acid, 28 mM sodium phosphate and 4 mM ammonium molybdate) in the sample vial. The blank solution contained 4 mL of the reagent solution. The vial was capped and incubated in a water bath at 95 °C for 90 min. After the sample was cooled to room temperature, the absorbance of the mixture was measured at 695 nm against the blank. The antioxidant activity was expressed relative to that of the BHT. All determinations were assayed in triplicate and mean values were calculated.

2.2.5.3. Ferric reducing antioxidant power (FRAP) assay. The FRAP assay was done according to the method reported earlier [23]. Briefly, stock solutions included a 300 mM acetate buffer (pH 3.6), a 10 mM TPTZ solution in 40 mM hydrochloric acid, and a 20 mM ferric chloride hexahydrate solution. The fresh working solution was prepared by mixing 25 mL of an acetate buffer, a 2.5 mL TPTZ solution and a 2.5 mL ferric chloride hexahydrate solution and then warmed to 37 °C before use. The plant sample solutions and control (Trolox) were prepared in methanol (250 μg/mL). 10 μL of each sample solution was taken in separate test tubes and 2990 μL of a FRAP solution was added to each to make a total volume up to 3 mL. The plant samples were allowed to react with the FRAP solution in the dark for 30 min. The absorbance of the colored product (ferrous tripyridyl triazine complex) was checked at 593 nm. The FRAP values were expressed as micromoles of Trolox equivalents (TE) by using the standard curve constructed for different concentrations of Trolox.

2.2.5.4. Lipid peroxidation inhibition assay by the ferric thiocyanate method (FTM). 0.1 mL of each sample solution (0.5 mg/mL) was mixed with 2.5 mL of the linoleic acid emulsion (0.02 M, pH 7.0) and 2.0 mL of a phosphate buffer solution (0.02 M, pH 7.0). The linoleic emulsion was prepared by mixing 0.28 g of linoleic acid, 0.28 g of Tween 20 as an emulsifier and 50.0 mL of a phosphate buffer. The reaction mixture was incubated for 5 days at 40 °C. The mixture without the extract was used as a control. The mixture (0.1 mL) was taken and mixed with 5.0 mL of 75% ethanol, 0.1 mL of 30% ammonium thiocyanate and 0.1 mL of 20 mM ferrous chloride in 3.5% HCl and was allowed to stand at room temperature. Precisely 3 min after the addition of ferrous chloride to the reaction mixture, the absorbance was recorded at 500 nm.

The antioxidant activity was expressed as the percent inhibition of peroxidation (IP%):

$$IP\% = \left(1 - \frac{(Abs\ of\ sample)}{(Abs\ of\ control)}\right) X100$$

The antioxidant activity of BHT was assayed for comparison as the reference standard. All the measurements were done in triplicate and statistical analysis was performed by Microsoft Excel 2010. The results are presented as the average ± SEM.

2.2.6. Enzyme inhibition assays

The overproduction of enzymes in the body causes many serious diseases, e.g., Alzheimer's disease which is a chronic neurological disorder. So, *in vitro* experiments were conducted to determine the inhibitory potential of ZnO-NPs against the enzymes: lipoxygenase, α-glucosidase, and butyryl cholinesterase.

2.2.6.1. α-glucosidase inhibition assay. The reaction mixture contained 70 μL of a 50 mM phosphate buffer saline with 6.8 and 10 μL (0.5 mM) of the test compound, followed by adding 10 μL (0.057 units) of the enzyme, thus, making a total volume of up to 100 μL. The contents were mixed thoroughly and incubated at 37 °C for 10 min. Then, a reading was taken at 400 nm. Then, 10 μL of a 0.5 mm substrate (*p*-nitro phenylglucosepyranose) was added to initiate the reaction. Acarbose was taken as a positive control. It was incubated for 30 min at 37 °C and then the absorbance was measured using a Synergy HT microplate reader at 400 nm. All readings were taken in triplicate. Percent inhibition was calculated by the following equation:

$$\text{Inhibition}\ (\%) = \frac{Control - Test}{Control} \times 100$$

2.2.6.2. Butyryl cholinesterase and acetylcholinesterase assay. The reaction mixture contained 60 μL (50 mM) of a Na_2HPO_4 buffer having a pH of 7.7 and 10 μL (0.5 mM well^{-1}) of the test compound, followed by adding 10 μL of BChE (0.5 unit well^{-1}), thus making a total volume of up to 100 mL. The contents were mixed thoroughly, and the absorbance was noted at 405 nm. Then, the reaction mixture was incubated at 37 °C for 10 min. Then, 10 μL (0.5 mM well^{-1}) of the substrate (butyryl thiocholine bromide) was added to initiate the reaction followed by adding 10 μL DTNB (0.5 mM well^{-1}). It was incubated for 30 min at 37 °C and then the absorbance was noted at 405 nm using a Synergy HT microplate reader. Serine (0.5 mM well^{-1}) was taken as the positive control. After 30 min of incubation at 37 °C, the absorbance was measured at 405 nm. A Synergy HT (Biotech, USA) 96-well plate reader was used in all experiments. All readings were taken in triplicate. Percent inhibition was calculated by the following equation:

$$\text{Inhibition}\ (\%) = \frac{1 - Abs.\ of\ test\ compound}{Abs.\ of\ Control} \times 100$$

2.2.6.3. Lipoxygenase inhibition assay. The reaction mixture contained sodium phosphate buffer, 140 μL (100 mM) having a pH of 8.0, 15 μL (600U) of a purified lipoxygenase enzyme (Sigma-Aldrich, USA) and 20 μL of a test compound, thus, making a total volume of up to 100 mL. The contents were mixed thoroughly, and absorbance was noted at 234 nm. It was incubated at 25 °C for 10 min. Then, 25 μL of the substrate solution was added to initiate the reaction. The absorbance change was noted at 234 nm after 6 min, using a Synergy HT (Biotech, USA) 96-well plate reader. Baicalein (0.5 mM well^{-1}) was taken as a positive control. Percentage inhibition was calculated by the following formula.

$$\text{Inhibition}\ (\%) = \frac{1 - Abs.\ of\ test\ compound}{Abs.\ of\ Control} \times 100$$

2.2.7. Antimicrobial activity

Antimicrobial activity was examined against a broad spectrum of microbes of skin diseases and acne as described below.

2.2.7.1. Antibacterial activity of ZnO-NPs. The antibacterial activity of ZnO-NPs pellets was tested by the disc diffusion method [15]. The bacterial species were collected from Dr. Nalla. G. Palaniswami, Department of Microbiology Lab, Arts and Science College, Coimbatore. The microorganisms used for the assay were *Proteus vulgaris, Staphylococcus aureus, E. coli, Pseudomonas aeruginosa,* and *Klebsiella pneumonia*. The antibacterial activity of the synthesized ZnO-NPs was evaluated by measuring the zone of inhibition.

For this, 4 mm discs were prepared using What-man No: 1 filter paper. The discs were obtained by punching and putting them in vials bottles and sterilizing them in an oven at 150 °C for 15 min. The disc was impregnated with 10 μL of a concentrated crude extract and another disc was impregnated with synthesized ZnO-NPs. The discs were evaporated at 37 °C for 24 h. The prepared discs containing the various fractions were carefully placed on the inoculated plates using sterilized forceps in each case. The antibiotic tetracycline was used as a control. The plates were then turned upside down and incubated at 37 °C for 24 h in an incubator. The results were taken by considering the growth and inhibition zone of the bacteria by the test fractions. The antibacterial activity was evaluated by measuring the diameter of the inhibition zone (IZ) around the disc.

2.2.7.2. Antibacterial assay against levofloxacin-resistant strains. Different pneumococcal strains were cultured in THY medium at 37 °C until reaching the stationary phase. The cultures were then harvested by centrifugation and washed with PBS two times and finally dispersed into 2 mL of THY to make a stock solution. Resuspended bacterial solution concentrations were then determined by optical density measured at 600 nm. A volume of 650 μL of the bacterial solution was added into a 1 mL tube and mixed with 150 μL of a NP solution. The NP concentration was varied by half according to a standard protocol, ranging from 0.11 μM to 0.8 nM. THY medium was used to make different dilutions. A control growth group without NPs and a negative control group with levofloxacin from 2.048 mM to 0.016 mM were carried out at the same time. Cultures were incubated for 24 h in triplicate, and at least two independent experiments were repeated on different days. The CFU was calculated by plating each dilution after further diluting them ten-fold. The MIC 90 is defined as the minimum concentration of ZnO-NPs that inhibits 90% of bacteria colonies as observed with the unaided eye on a blood plate.

2.2.7.3. Calculation of IC_{50} values. IC_{50} values (i.e., concentrations that cause 50% inhibition of the enzyme) for the samples were measured by using EZ-Fit Enzyme Kinetic Software (Perrella Scientific Inc., Amherst, USA).

2.2.8. In vivo toxicological profiling of ZnO NPs

A 14 day multiple dose toxicity evaluation was conducted to determine the fate and response of ZnO-NPs in mice. The animal procedures were conducted as per approved guidelines from a research ethical committee at Riphah International University. The animals were divided into 2 groups, i.e. A and B (n = 6), and were kept under a controlled environment with free access to food and water. Group A was given 100 μg ZnO-NPs in WFI through an i.v. using a sterile syringe. Group B was given simple WFI through an i.v. The same treatment was repeated for 14 days with an alternate day dose administration. The animals were carefully monitored for any changes in body weight, activity, and evident changes. After 14 days, the blood was collected *via* cardiac puncture for biochemical evaluation. The mice were euthanized and the liver, kidney, heart, and lungs were removed, washed with buffer and stored in 10% formalin for histopathological evaluation [24].

2.2.9. Statistical analysis

The results were statistically analyzed to determine the significant differences between the data. The data are presented as mean ± SD and mean ± SEM. Moreover, one-way and two-way ANOVA were used to analyze the data using the Graph pad prism software version 7.0. $*P < 005$, $**P < 0.01$ and ***P < 0.001 were considered as significant, moderately significant and highly significant results, respectively.

3. Results

3.1. Synthesis of the plant extract based ZnO NPs

The plant extract was carefully extracted, dried and stored in a container. The ZnO-NPs using the Neem extract were prepared with an average particle size of 21.39 ± 1.58 nm with a zeta potential of −23.6 ± 2.8 and PDI 0.383.

3.2. ICP-MS, FTIR and XRD analyses

ICPMS revealed 0.81 mg of Zn in 1 mg of a dried ZnO-NPs sample. The FTIR spectra of the plant extract and ZnO-NPs are shown in Fig. 1, which clearly indicate the peaks were shifting and bending in specific regions confirming the synthesis of ZnO-NPs. The XRD analysis was done to study the nature and particle size of the ZnO-NPs as shown in Fig. 2. The average particle size measured using XRD data was found to be 19.57 ± 1.56 (Table 1).

3.3. Scanning electron microscopy

Scanning electron microscopy (SEM) was used to identify the morphology and size of the nanoparticles. The SEM image (Fig. 3) shows the successful synthesis of high-density ZnO-NPs from the *Azadirachta Indica* plant extract. The morphology of the ZnO-NPs was found to be non-spherical with average particle sizes around 20 nm, which might of great interest as an antibacterial agent.

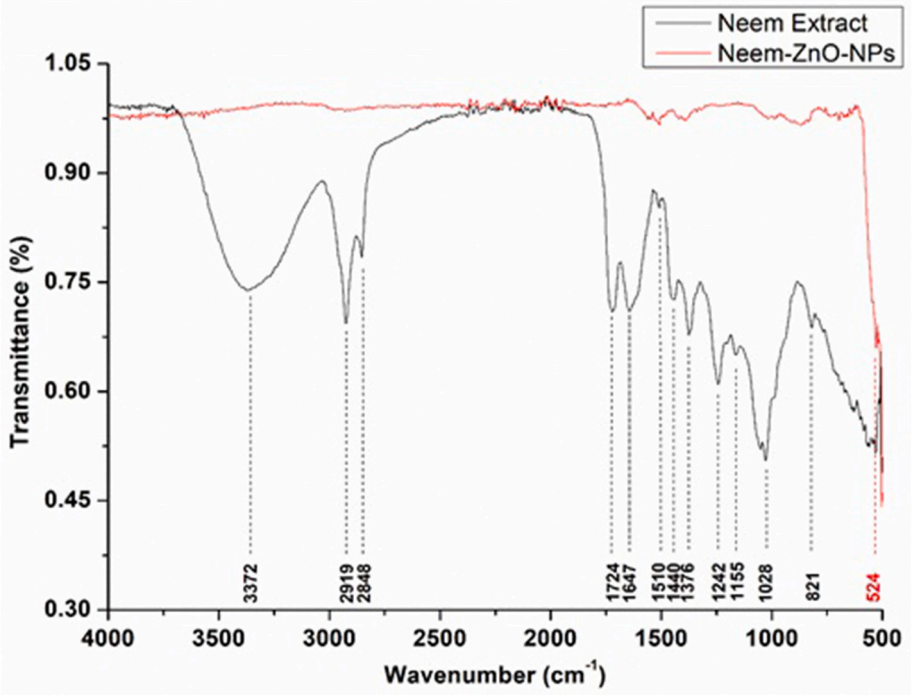

Fig. 1. FTIR spectra of ZnO-NPs and Neem extract showing characteristic peaks over the wave numbers 500–4000.

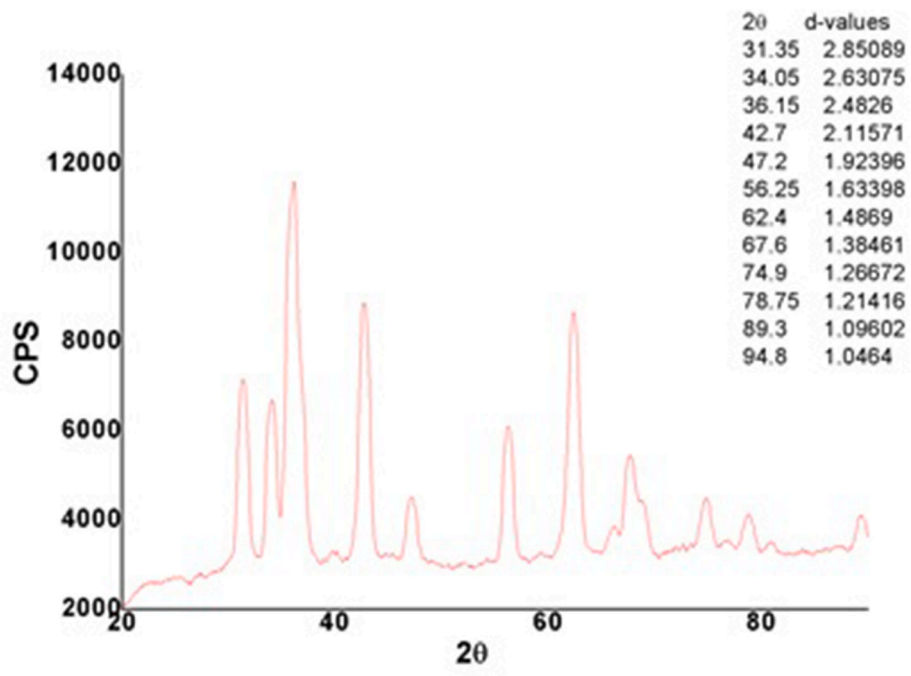

Fig. 2. XRD spectra of ZnO-NPs showing characteristic peaks of the dry formulation over a 2Θ range of 20–80 used to calculate the particle size of ZnO-NPs.

Table 1
Particle size of ZnO-NPs calculated using XRD data.

S. No.	2θ	θ_2-θ_1 at f.w. h.m.	B (radians)	Grain size (nm)	Av. grain size (nm)
1.	36.15	0.42	0.0075	19.4	19.57 ± 1.56
2.	34.05	0.42	0.0075	19.3	
3.	31.35	0.43	0.0075	19.2	
4.	56.25	0.44	0.0077	20.4	

3.4. Antioxidant activity

The percent scavenging of the green synthesized ZnO-NPs was measured, and the results are shown in Table 2. It was observed that ZnO-NPs showed a moderate percent scavenging as compared to the standard reference 3,5-di-tert-4-butylhydroxytoluene (BHT) which showed 95.19 ± 1.12% scavenging of the DPPH radical at a concentration of 500 μg/mL, whereas, similar scavenging was achieved by BHT at a concentration of 60 μg/mL. The FRAP assay showed very good values for ZnO-NPs (275 ± 0.48 TE μM/mL) as compared to blanks (18.63 TE μM/mL). This higher FRAP value indicates the high antioxidant potential of the ZnO-NPs. ZnO-NPs inhibited lipid peroxidation and percent inhibition was 46.87 ± 1.42%. Although this activity was slightly lower than the standard BHT (62.48 ± 1.07%), the lipid peroxidation potential of ZnO-NPs was evident. All of these results suggest that ZnO-NPs are effective inhibitors of reactive oxygen species with a broad spectrum of activity.

3.5. Enzyme inhibition potential

ZnO-NPs displayed good activity against the α-glucosidase enzyme (Table 3). It showed comparable inhibition of 82.77 ± 0.64% as compared to the reference standard serine (89.75 ± 0.32%). IC_{50} values were 72.58 ± 0.93 μg/mL and 84.09 ± 0.24 μg/mL for the ZnO-NPs and serine, respectively. ZnO-NPs did not show considerable activity against butyryl cholinesterase (Table 3). It showed only 34.59 ± 0.62% inhibition as compared to a reference standard, Baicalein, which showed 91.65 ± 0.27% inhibition. ZnO-NPs showed moderate inhibition activity against lipoxygenase, i.e. 66.39 ± 0.12%, as compared to a reference standard acarbose which showed 91.23 ± 0.43% inhibition. IC_{50} values for ZnO-NPs was 89.83 ± 0.45 μg/mL and that of acarbose was 39.15 ± 0.17 μg/mL as shown in Table 3. The results indicated a slightly decreased lipoxygenase inhibition as compared to the standard, yet did possessed inhibitory potential.

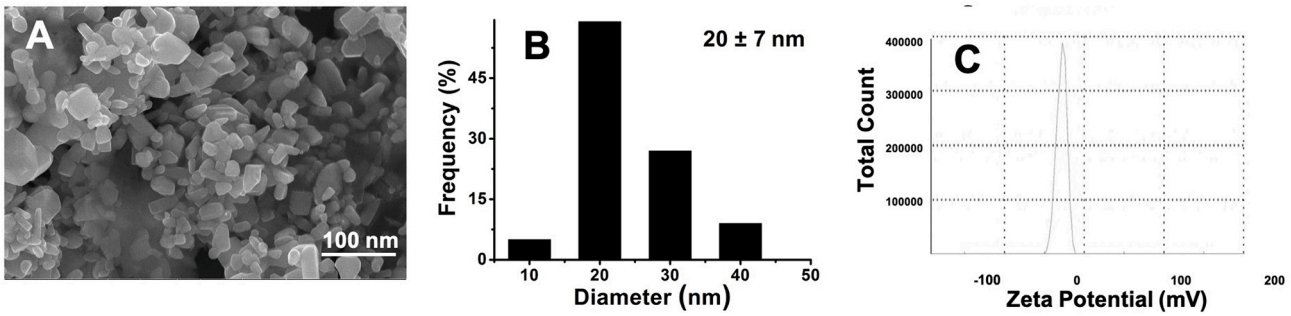

Fig. 3. Scanning electron microscopic (SEM) analysis of ZnO-NPs showing particles with non-spherical morphology with varying size distribution (A), size distribution by ImageJ software (B) and zeta potential distribution by a Zetasizer (C).

Table 2
DPPH radical scavenging activity, results are shown as mean ± SEM of three assays.

Sr. No.	Sample	Conc. in assay μg/mL	% Scavenging of DPPH radical
1	ZnO-NPs	500	95.19 ± 1.12***
		250	72.25 ± 0.8***
		120	57.30 ± 0.34***
		60	34.00 ± 0.67
2	Butylated hydroxytoluene (BHT)	60	94.35 ± 0.14
		30	78.46 ± 0.08
		15	46.57 ± 0.0
		8	25.47 ± 0.34

***P < 0.001 level of significance was given in comparison to the 60 μg/mL concentration.

3.6. Antibacterial activity

The zone of inhibition experiments were measured in mm and results are given in Table 4. It was observed from the results that at a concentration of 100 μL (0.72 mg/mL, w/v), ZnO-NPs showed moderate activity. The zone of inhibition values were 11 mm, 13 mm, 13 mm and 10 mm for *S. pyogenes*, *B. subtilis*, *S. aureus*, and *E. coli*, respectively, at 100 μL (0.72 mg/mL, w/v) as compared to methicillin which showed 17 mm, 20 mm, 23 mm and 16 mm zone of inhibition values for *S. pyogenes*, *B. subtilis*, *S. aureus*, and *E. coli*, respectively, at 100 μL concentrations. As the concentration of ZnO-NPs increased, the antibacterial activity also increased. It displayed very good antibacterial activity at a 500 μL (0.72 mg/mL, w/v) concentration, i.e. 17 mm, 24 mm, 23 mm and 18 mm zone of inhibition values for *S. pyogenes*, *B. subtilis*, *S. aureus*, and *E. coli*, respectively.

3.7. Activity against a levofloxacin resistant strain

The results of the antibacterial effect of ZnO-NPs against levofloxacin resistant (5203-23) and susceptible (D-39, Tigr-4, 63803) pneumococcal strains are shown in Table 5. The results clearly showed that the MIC-90 value of the ZnO-NPs was quite low against all four pneumococcal strains as compared to levofloxacin. In Fig. 4d, on a blood plate, the colonies of pneumo can be seen clearly growing in controls and other concentrations except for the first one (MIC-90). Different concentrations of ZnO-NPs and levofloxacin prepared by the serial dilution method (Fig. 4e) were used for determining the MIC.

3.8. In vivo toxicological profiling of ZnO-NPs

The toxicity of ZnO-NPs was evaluated in mice for 14 days at a relatively higher dose of 200 μg through i.v. administration on alternate days. For 14 days, the mice did not show any visible signs of toxicity, like a decrease in body weight, changes in feces or any other sign. The average body weight (n = 6) of the control and treatment group was 31.43 g and 31.98 g, respectively, which increased to 33.76 g and 35.44 g, respectively, showing normal metabolism and animal function resulting in progressive animal growth. The organ to body weight index showed no significant difference. The serum biochemistry analysis based on liver functional tests and renal functional tests are shown in Table 6. The results of these parameters showed some deviations as compared to the reference values and control groups. The complete blood picture, as shown in Table 7, did not show any significant change in the levels of different blood components; thus indicating no toxicity of ZnO-NPs towards blood. The histopathology of vital organs (liver, kidney, and lungs) is shown in Fig. 5 and also suggested the biocompatibility of the ZnO-NPs as no microscopic changes were observed in the tissues of these organs.

4. Discussion

The green synthesis of A*zadirachta indica* (Neem) extract assisted zinc oxide nanoparticles (ZnO-NPs) was successfully carried out and was confirmed through UV-spectroscopy. The prepared white ZnO-NPs were

Table 5
Antimicrobial activity of ZnO-NPs against different levofloxacin sensitive and resistant strains; all results are presented as mean ± SEM of three assays.

Formulation	D-39 MIC	Tigr-4 MIC	63803 MIC	5203-23 MIC
Levofloxacin (mM)	0.51 ± 0.38	1.02 ± 0.29	1.02 ± 0.34	2.08 ± 0.15
ZnO-NPs (nM)	3.48 ± 0.49***	3.48 ± 0.46***	6.90 ± 0.42***	14.6 ± 0.13***

***P < 0.001 was given when compared to Levofloxacin.

Table 3
Enzyme inhibition activities of ZnO-NPs against lipoxygenase, α-glucosidase and butyryl cholinesterase (BchE). All results are presented as mean ± SEM of three assays.

Sample	Lipoxygenase activity		α-Glucosidase activity		BchE activity	
	%Inhibition (0.1 mg/mL)	IC_{50} (μg/ml)	%Inhibition (0.1 mg/mL)	IC_{50} (μg/ml)	%Inhibition (0.1 mg/mL)	IC_{50} (μg/ml)
ZnO-NPs	66.39 ± 0.12	89.83 ± 0.45	82.77 ± 0.64	72.58 ± 0.93	34.59 ± 0.62	NIL
Acarbose	91.23 ± 0.43	39.15 ± 0.17	–	–	–	–
Serine	–	–	89.75 ± 0.32	84.09 ± 0.24	–	–
Baicalein	–	–	–	–	91.65 ± 0.27	23.10 ± 1.90

Table 4
Zone of inhibition of ZnO-NPs against different bacterial strains.

Bioactive Agent		Zone of Inhibition[a] (Diameter, mm)			
		Streptococcus pyogenes	Bacillus subtilis	Staphylococcus aureus	Escherichia Coli
ZnO-NPs[a]	100 μL	11 ± 0.6	13 ± 1.3	13 ± 0.9	10 ± 1.3
	200 μL	12 ± 1.2	17 ± 0.7	16 ± 0.5	11 ± 0.7
	300 μL	14 ± 0.9	19 ± 0.9	18 ± 0.4	15 ± 0.4
	400 μL	15 ± 0.1	21 ± 0.2	20 ± 0.7	16 ± 0.6
	500 μL	17 ± 0.8	24 ± 0.4	23 ± 1.6	18 ± 1.4
Methicillin	100 μL	17 ± 0.5	20 ± 0.7	23 ± 0.3	16 ± 0.1

[a] Inhibition zone (mm) includes the diffusion assay disc diameter (6 mm), which carried 50 μL from the ZnO−NPs suspension. The diameters of the inhibition zones are mean±standard deviation in triplicate.

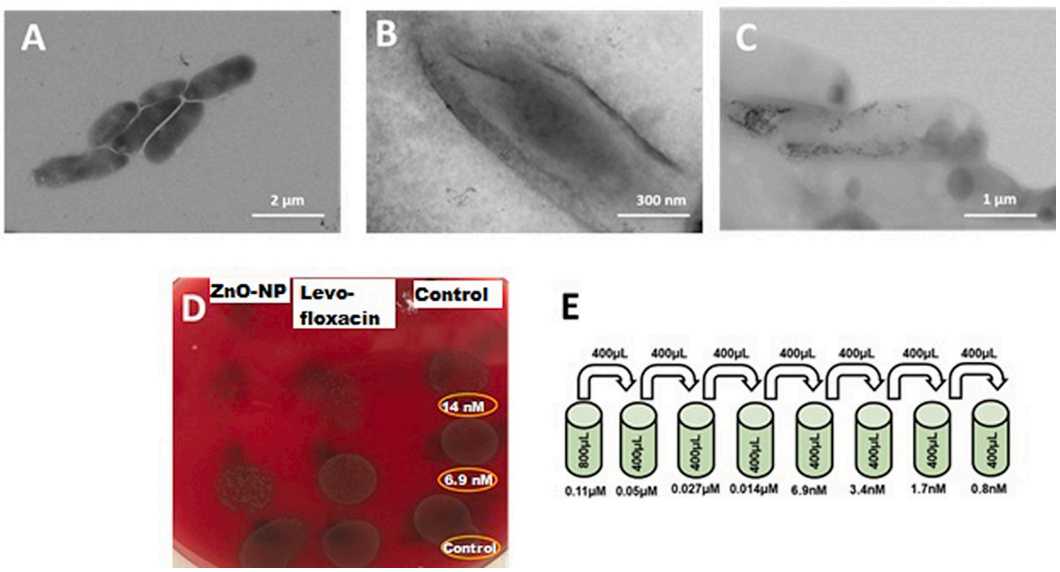

Fig. 4. (A) Scanning electron microscopic (SEM) images of bacterial controls; (B & C) SEM images of bacteria after ZnO-NP treatment showing a clear accumulation of ZnO-NPs inside the bacteria; (D) petri dish showing pneumococcal strains cultured in THY medium at 37 °C after 24 h of incubation with different concentrations of NPs and Levofloxacin and (E) dilutions used for antibacterial activity of different ZnO-NPs and levofloxacin.

Table 6
Various biochemical parameters evaluated for 14 days of treatment with ZnO NPs, compared to the control mice group. The results are presented as the mean ± S.D of three experiments.

Parameter	Unit	Reference values	Control	ZnO-NPs
ALT	U/L	10–40	24.66 ± 0.34	42.36 ± 1.78***
ALP	U/L	65–306	156.28 ± 0.49	190.66 ± 5.09***
AST	U/L	10–40	36.46 ± 1.01	43.34 ± 4.28*
Total Protein	g/dL	4.5–6.5	3.82 ± 0.26	4.08 ± 0.33
Total Bilirubin	mg/dL	0.2-1.0	0.58 ± 0.06	0.77 ± 0.06
Uric Acid	mg/dL	4–7	5.02 ± 0.09	8.83 ± 1.13**
Urea	mg/dL	10–50	22.63 ± 0.73	31.84 ± 4.37**
Creatinine	mg/dL	0.5-1.3	0.54 ± 0.04	0.62 ± 0.03

*P < 0.05, **P < 0.01 and ***P < 0.001 level of significance was given when compared to the control.

Table 7
Complete blood profiles of control and ZnO-NPs treated group after 14 days, shown as mean ± SD of three independent results.

CBC	Unit	Control	ZnO-NPs
Hb	g/dL	12.56 ± 0.44	14.60 ± 0.49
TLC	x 10^9	7.80 ± 0.21	5.40 ± 0.35
RBC	x 10^{12}/L	6.49 ± 0.23	7.48 ± 0.34
HCT	%	35.83 ± 0.41	44.42 ± 0.52
MCV	Fl	56.56 ± 0.58	59.71 ± 0.35
MCH	Pg	18.93 ± 0.57	18.38 ± 0.57
MCHC	%	34.96 ± 0.20	32.40 ± 0.44
Platelets	x 10^9/L	1056 ± 98.30	1135 ± 36.57
Neutrophils	%	3.33 ± 0.94	4.33 ± 0.47*
Lymphocytes	%	83.00 ± 4.54	78.66 ± 3.29
Monocytes	%	4.33 ± 0.94	8.33 ± 0.47*
Eosinophil	%	2.33 ± 0.47	3.33 ± 0.47*

*P < 0.05 was given in comparison to the control.

stored in a well-closed container.

Plant mediated green synthesis of nanoparticles is a widely accepted biomimetic process for the large-scale production of biocompatible and biodegradable nanoparticles. This technology is simplified, rapid, reproducible and developed by using bioresources. Plants employed in this technique are usually naturally and abundantly available in the normal flora hence making the green synthesis of nanoparticles a cost-effective process. The green biosynthesis of nanoparticles is essentially important as it is free from any physical and chemical contamination. The methodology followed here is also free from the utilization or generation of any hazardous substances.

Unlike other plants, such as *Acalypha indica*, where additional reducing agents like caffeine and theophylline are required, terpenoids and flavanones are naturally occurring phytochemicals in Neem leaves and act as reducing agents. Moreover, these phytochemicals also play an essential role as capping agents helping to stabilize the nanoparticles [25]. *Azadirachta indica* from the Meliaceae family is commonly available in Indo-Pak regions. Leaves of this plants along with other parts are also commonly used as many household remedies for fungal and bacterial infections. The Neem leaf powder is used to improve gut heath, boost immunity and remove body toxins. In addition to the very cost-effective, natural and indigenous availability of the Neem plant, it can provide the bioconversion of nanoparticles form its counterparts at relatively lower concentrations and without using any additional physical or chemical agents. Moreover, it has been reported that it is indeed a fast reducing agent with a rapid formation of nanoparticles [3]. A broad range of various phytochemicals in the Neem leaf extract exhibit reducing properties that result in the fast bioreduction of zinc ions into nanoscaled ZnO particles. Water soluble phytochemicals (such as flavones, organic acids and quinones) are more likely to be involved in this bioconversion. Additionally, it has been reported that the average particle size of nanoparticles decreased by quinone activation through the incubation process of benzoquinones present in Neem [4].

The reducing and capping capability of the A*zadirachta indica* extract was established from comparative FTIR analysis of ZnO-NPs and that of the extract. The FTIR spectrum of the extract (Fig. 1) showed characteristic peaks appearing at 3372 and 2919 cm^{-1}, which are attributed respectively to O–H stretching and C–H bending vibrations, and this indicates the presence of alcohols. The broadened band between 3300 and 3500 cm^{-1} is assumed due to overlapping of N–H and O–H

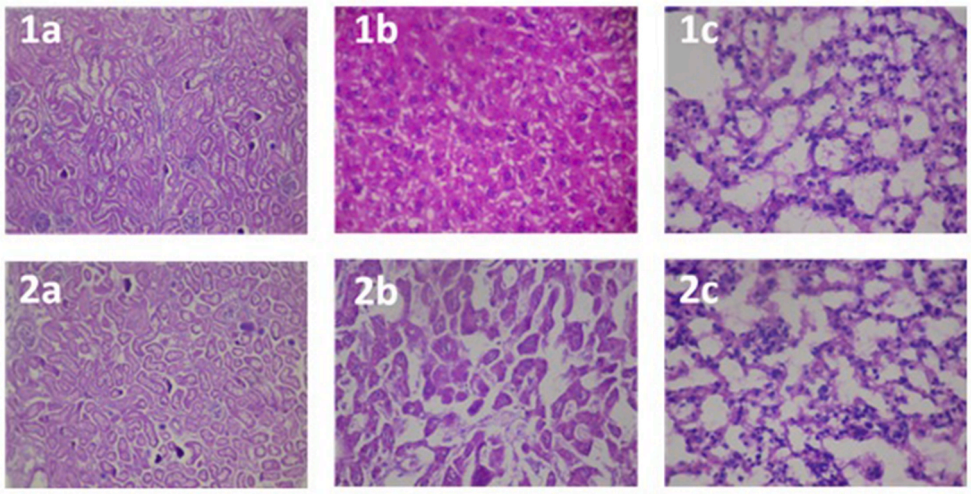

Fig. 5. Histopathology of organs: (1a) Control kidney, (2a) ZnO NPs treated kidney, (1b) Control liver, (2b) ZnO NPs treated liver, and (1c) Control lungs, (2c) ZnO NPs treated lungs. The images are taken at a 40 X optical zoom.

stretching vibrations. The peaks appearing at 1724 and 1647 cm^{-1} are recognized as a –C═O stretching vibration accredited respectively to the presence of carboxylic and amide or amine groups in the plant extract. The –C–O– stretching peaks observed at 1155 cm^{-1} are due to the presence of terpenoids and flavonoids in the plant extract [3]. The suppression in intensity or disappearance of peaks in the FTIR spectrum of ZnO NPs at 3372, 1724 and 1647 cm^{-1} indicates the involvement of carboxylic, amide and carbonyl moieties with ZnO-NPs. The sharp peak for the Zn–O stretch appeared below 500 cm^{-1} having a weak band positioned at 524 cm^{-1} and is ascribed to the ZnO-NPs [26]. Inductively coupled plasma-mass spectrometry (ICP-MS) has become an imperative estimation technique for determining the chemistry of inorganic nanoparticles in samples [27]. The results from ICP-MS revealed 0.91 mg of Zn in 1 mg of the ZnO-NP sample. The XRD analysis of the ZnO-NPs is shown in Fig. 2. A definite line broadening of the XRD peaks indicates that the prepared material is comprised of nanosized particles.

The crystalline form of the prepared ZnO nanoparticles was hexagonal-wurtzite, and this was confirmed by analyzing the XRD data of our particles with HighScore X'Pert Plus software. The XRD diffraction patterns appearing at 2θ values of 31.35, 34.05, 36.15, 42.7, 47.2, 56.25, and 62.4 were in accordance with that of the hexagonal-wurtzite crystalline structure of ZnO (JCPDS card No: 36–1451) as explored/confirmed by HighScore X'Pert Plus software. From the XRD spectrum, the peak intensity, position, width, and full-width at half-maximum (f.w.h.m.) were calculated. Using the Debye-Scherrer equation, the particle size of ZnO was found to be 19.57 ± 1.56 nm, derived from the more intense peak corresponding to the plane located at 36.15°. The size obtained from XRD is close to what was calculated through DLS (21.39 ± 1.58 nm). The size distribution histogram is shown in Fig. 3B and the zeta potential curve is show in Fig. 3C.

During metabolic processes in the body, free radicals are produced. The overproduction of free radicals during pathological conditions leads to oxidative stress that might result in many serious diseases, such as heart diseases, cancer, inflammation, diabetes, and neuro-degenerative diseases, etc. So, antioxidants are helpful in preventing such problems [8,28]. Keeping in mind the importance of antioxidants, the *in vitro* antioxidant potential of the green synthesized ZnO-NPs was assessed through different methods: 1) 1,1-diphenyl-2-picrylhydrazyl radical (DPPH) scavenging, 2) the total antioxidant activity by phosphomolybdenum complex method, 3) a FRAP assay, and 4) a ferric thiocyanate assay in comparison with standard reference antioxidants. DPPH is a stable free radical and gives a purple color to the solution. The reaction takes place between DPPH radicals and antioxidant molecules which can be observed by a decrease in purple color or absorbance during spectrophotometry. The percent scavenging increases linearly as the concentration of the antioxidant sample is increased during the reaction [28]. The IC_{50} value of the ZnO-NPs was 116.05 ± 1.80 μg/mL, as compared to BHT which had an IC_{50} value of 12.32 ± 0.87 μg/mL. However, when ZnO-NPs were compared with their lowest concentration, higher concentrations of ZnO-NPs showed a significant increase in percent scavenging potential ($P < 0.001$).

Reactive oxygen species (ROS) (e.g., hydroxyl radicals, hydroperoxide radicals, etc.) cause serious oxidative effects. These can be measured easily by the FRAP assay. ZnO-NPs reduce such reactive species by donating electrons. Fe^{3+} is reduced by ZnO-NPs to Fe^{2+} which forms a complex with tripyridyltriazine (TPTZ). A complex shows a dark blue color having a maximum absorption at 593 nm [29]. The ZnO-NPs showed a 13-fold superior ROS scavenging ability compared to a standard compound, which might be of great interest.

Lipid peroxidation is a key step in the pathogenesis of ROS. The reaction takes place between ROS and the unsaturated double bonds which results in the formation of toxic hydroperoxides in the system. The lower the peroxide level, the lower the oxidative damage. We assumed that ZnO-NPs can react with lipid peroxy radicals and convert them to a reduced form to inhibit the generation of new radicals [30]. Therefore, the antioxidant activities of various fractions of the ZnO-NPs were tested to inhibit peroxidation of the model unsaturated lipid, linoleic acid, by the ferric thiocyanate method (FTM) [31]. The results obtained were comparable to the standard used in the assay. All these antioxidant assays showed impressive ROS scavenging and antioxidant potential of ZnO-NPs.

ZnO-NPs successfully showed inhibition of different enzymes associated with metabolic disorders. α-glucosidase is involved in the breakdown of complex carbohydrates to yield glucose and its inhibition is desired in some metabolic diseases like diabetes mellitus type 2. Therefore, α-glucosidase inhibition activity was examined using the previously reported method [32]. Cholinesterase enzymes are involved in the metabolism of the neurotransmitter acetylcholine. Inhibition of cholinesterase is desired to increase the level of acetylcholine in many diseases such as Alzheimer's disease and myasthenia gravis [33]. Lipoxygenase (LOX) is involved in the production of inflammation mediators, leukotrienes, and their inhibition is required in the management of chronic inflammatory diseases. LOX inhibition activity was evaluated by a slightly modified standard method [34]. The enzyme inhibition activity of ZnO-NPs against all these enzymes showed significant lower ($p < 0.05$) IC_{50} values as compared to the reference compounds (Table 3).

Both the size and shape of the ZnO-NPs play a vital role in controlling their antibacterial activity. ZnO-NPs have been reported for their superior antibacterial activity with smaller size particles. This might be due to better cellular internalization of the NPs and/or accumulation at the cell membrane resulting in cell death [35]. Similarly, the morphology of the ZnO-NPs has an influence on its bactericidal potential. Rod-shaped ZnO-NPs have better cellular penetration resulting in higher bacterial killing as compared to spherically shaped NPs. Moreover, flower-shaped particles have been reported to have superior bactericidal activity as compared to both rod and spherical shapes [15].

Morphology dependent antibacterial activity is determined in terms of active facet percentages in ZnO-NPs, e.g. rod and spherical shaped ZnO-NPs have 111 and 100 active facets, respectively. The high atom density facets in 111 leads to superior antibacterial activity. Thus, the morphology can influence the antibacterial potential as the rod-or wire shaped ZnO-NPs have better cellular penetration and higher active facets resulting in higher bacterial killing as compared to spherical shaped ZnO-NPs. Moreover, it is suggested that the higher number of polar facets of ZnO-NPs possess higher quantities of oxygen vacancies which increase ROS generation resulting in better antibacterial activity [15,16]. Therefore, the hexagonal shaped ZnO-NPs reported here, would have superior antibacterial activity against resistant bacterial strains as compared to that already reported by other shapes.

It is well established that bacteria develop resistance against antibiotic drugs, so there is certainly a need to discover and produce new antibacterial drugs. Keeping in view this importance, the green ZnO-NPs (size- 20 nm) fabricated here were assessed for their antibacterial potential against bacterial species including gram-positive bacteria, i.e. *Streptococcus pyogenes*, *Bacillus subtilis* and *Staphylococcus aureus*, and 1 g-negative bacteria, i.e. *Escherichia coli*, by the disc diffusion method using methicillin, a standard antibiotic, as a positive control [36,37]. [35,36] The results showed superior antibateral potential of ZnO-NPs against these bacteral strains as compared to methicillin. Moreover, the antibacterial activity against levofloxacin sensitive and resistant strains was also evauated. Metal-based NPs have been reported to interact and block various metabolic pathways in bacteria owing to their ability to target prokaryotic cells through metal transport channels and metalloproteins, thus, killing multi drug-resistant bacteria. The bactericidal effect is mainly achieved through three distinct mechanisms: 1) interaction with the phospholipid bilayer, 2) binding to cytosolic proteins and 3) generation of reactive oxygen species (ROS), resulting in the structural and metabolic imbalance in a bacterial cell leading to cell death [37,38]. The ZnO-NPs formulated here significantly increased ($P < 0.001$) in activity as compared to levofloxacin in normal as well as resistant strains. This increased activity can be attributed to the antibacterial potential of ZnO-NPs due to polyhedral morphology. The SEM images of bacteria treated with ZnO-NPs (Fig. 4 b and c) clearly showed the attachment of small ZnO-NPs to the surface resulting in structural changes owing to the generation of ROS and production of pores in the bacteria membrane indicating a possible mechanism of cell death. ZnO-NPs have been reported as safe and biocompatible to human cells, which supports their potential use in the field as an antimicrobial agent at the appropriate concentration [15]. The exact mechanism is not yet clear but selective uptake of ZnO-NPs by prokaryotic cells *via* metalloproteins and metal transport channels may be responsible for their antibacterial activity [39]. The use of *A. indica* as a stabilizing agent for ZnO-NPs synthesis was also specifically employed for the treatment of acne *via* topical application through an ointment. The *A. indica* has proven its efficiency against various diseases because of the presence of phytochemicals and enzymes that act as antibacterial agents. This could further potentiate the antibacterial efficiency against various skin diseases.

The acute toxicity of ZnO-NPs was evaluated following *OECD 425* in a mouse model. The evaluation of the toxicity of new drugs is mandatory to identify a safer drug range to monitor their clinical outcomes [40]. The toxic potential of drugs on vital body organs is measured in terms of clinical signs and symptoms which are prime observations. The change in body weight index is a key indicator to evaluate induced toxicity, which did not show a significant difference from the control group (Fig. 5). The mortality rate was zero during the study duration with some behavioral patterns monitored during the first 24 h of dosing. Lacrimation and itching was present during the first 4 h and may be due to lacrimal obstruction, reflex tearing and abnormal position of the eyelid [41]. Biochemical evaluation based upon liver function tests (LFTs), renal function tests (RFTs), and complete blood counts (CBC) was investigated to examine the fate and effect of ZnO-NPs on these parameters after 14 days.

The tissue-damaging enzymes of the liver (Table 6), like ALT, were found to be higher in the ZnO-NP treated group than those in the normal group ($P < 0.001$). ALP is the hydrolase enzyme responsible for the destruction of proteins and removing of phosphate from the nucleotides [42]. ALP was also slightly higher in the treated group but remained within the normal range. This increase showed the cell-damaging effect of the ZnO-NPs at higher doses. Uric acid is the by-product of purine metabolism and an increased level of urea and uric acid indicate the destruction of cells and proteins [43]. ZnO-NPs treated mice had a moderately significant increase in urea and uric acid levels at the 14th day of treatment ($P < 0.01$). Oxidative stress causes the imbalance between pro-oxidant and antioxidant ratios. This increase causes the depletion of endogenous antioxidants that encourage the production of ROS leading to tissue damage and necrosis [44]. Any changes in hematological parameters (RBCs, WBCs, platelets, etc.) after the administration of ZnO-NPs were also analyzed. Neutrophil, monocytes and eosinophil counts significantly increased in ZnO-NP treated mice in comparison to the control ($P < 0.05$). Other hematological parameters had no significant difference between the control and treated groups with ZnO-NPs (Table 7). A previous study on the toxicology of ZnO-NPs revealed that zinc induces the production of pro-inflammatory mediators (cytokines) and its accumulation in cells associated with organellar clumping causes the release of Ca^{+2}, mitochondrial injury, and cytotoxicity [39,45,46]. The accumulation of ZnO-NPs into the cell make it beneficial for targeted drug delivery systems. They can also easily penetrate into the inflamed cell which is an advantage for targeted drug delivery systems. All of these parameters suggest that at higher doses, ZnO-NPs might show some dose-dependent toxicity towards the liver that may be addressed by decreasing the dose.

Histopathological changes in the kidney, liver, and lungs were microscopically examined and are shown in Fig. 5. The control and ZnO-NPs treated histopathological images of the kidney are illustrated in Fig. 5 (1a & 2a), respectively. Very slight swelling in the renal glomerulus was observed in the ZnO-NPs treated section of the kidney (Figs. 5–2a). This might also support slight changes in the RFT results described earlier. The liver histopathology of the ZnO-NP treated group indicated hydropic degenerative changes along with fatty changes (Figs. 5–2b). Hepatocytes were not intact with each other as the control group and minute necrotic cells were also observed. The histopathological image of the lungs showed no structural change in the ZnO-NP treated group as compared to the control group. Alveolar septal thickening was normal, and no neutrophils were observed in the interstitium (Figs. 5–2c). The overall toxicity evaluation suggested decent compatibility of ZnO-NPs after 14 days of toxicity evaluation [24].

Lastly, ZnO-NPs prepared by green synthesis using various plants have manifested promising antimicrobial activities. ZnO-NPs synthesized from *Azadirachta indica* exhibited significant antibacterial activity particularly against various antibiotic resistant bacterial strains. Moreover, ZnO-NPs proved their efficacy as free-radical scavengers and enzyme inhibitors against multiple metabolic disorders. Convincingly, these activities of ZnO-NPs are favorable towards the development and application of these nanoparticles for many applications paving the way for their practice as an alternative and safe treatment [47].

5. Conclusion

The results reveled that non spherically shaped, green ZnO-NPs synthesized *via* green Neem extracts displayed excellent broad spectrum antimicrobial activity against several Gram positive and negative microbes along with significantly superior activity against levofloxacin resistant pneumococcal strains. Besides these, the ZnO-NPs showed decent antioxidant activity and enzyme inhibition potential. *In vivo* toxicity evaluation revealed some changes in biochemical parameters after 14 days of treatment, yet, these were not that alarming suggesting the biocompatibility of ZnO-NPs up to a certain level. In short, the green ZnO-NPs with strong antioxidant, enzyme inhibition, and antimicrobial activities have great potential to be developed as a novel therapeutic agent for multifaceted biomedical applications.

Author contribution

Muhammad Farhan Sohail: Study conception, major experiments and over all supervision of the project, final editing and review of the manuscript.

Mubashar Rehman: Study designing, synthesis, manuscript writing and proof reading.

Syed Zajif Hussain: Scanning electron microscopic analysis and manuscript writing.

Zil e huma: Supported conducting *in vivo* studies and analysis.

Gul Shahnaz: In vivo experiments, manuscript proof reading.

Omer Slaman: Supported in formulation optimization and synthesis along with the provision of a few chemicals.

Shahper Mirza: Cell line studies and manuscript proof reading.

Qandeel Khalid: Formulation, drug release evaluation and proof reading of manuscript.

Irshad Hussian: Study conception and overall supervision of the project and final review of the manuscript.

Thomas J. Webster: Overall supervision of the project, statistical analysis, final review and editing of the manuscript.

Declaration of competing interest

The authors declare no conflict of interest.

Acknowledgments

The authors are grateful to Chughtai Labs Lahore for the provision of the levofloxacin resistant bacterial strains.

References

[1] J.R. Schwartz, R.G. Marsh, Z.D. Draelos, Zinc and skin health: overview of physiology and pharmacology, Dermatol. Surg. 31 (2005) 837–847.
[2] S. Iravani, Green synthesis of metal nanoparticles using plants, Green Chem. 13 (10) (2011) 2638–2650.
[3] S. Ahmed, et al., Green synthesis of silver nanoparticles using Azadirachta indica aqueous leaf extract, J. Radiat. Res. Appl. Sci. 9 (1) (2016) 1–7.
[4] T. Bhuyan, et al., Biosynthesis of zinc oxide nanoparticles from Azadirachta indica for antibacterial and photocatalytic applications, Mater. Sci. Semicond. Process. 32 (2015) 55–61.
[5] S. Kamble, et al., Evaluation of curcumin capped copper nanoparticles as possible inhibitors of human breast cancer cells and angiogenesis: a comparative study with native curcumin, AAPS PharmSciTech 17 (5) (2016) 1030–1041.
[6] M. Ovais, et al., Biosynthesized colloidal silver and gold nanoparticles as emerging leishmanicidal agents: an insight, Nanomedicine 12 (24) (2017) 2807–2819.
[7] A.K. Mittal, Y. Chisti, U.C. Banerjee, Synthesis of metallic nanoparticles using plant extracts, Biotechnol. Adv. 31 (2) (2013) 346–356.
[8] T.F. Alves, et al., Association of silver nanoparticles and curcumin solid dispersion: antimicrobial and antioxidant properties, AAPS PharmSciTech 19 (1) (2018) 225–231.
[9] A. Nadhman, et al., PEGylated silver doped zinc oxide nanoparticles as novel photosensitizers for photodynamic therapy against Leishmania, Free Radic. Biol. Med. 77 (2014) 230–238.
[10] S. Ahmed, S.A. Chaudhry, S. Ikram, A review on biogenic synthesis of ZnO nanoparticles using plant extracts and microbes: a prospect towards green chemistry, J. Photochem. Photobiol. B Biol. 166 (2017) 272–284.
[11] L.C. du Toit, et al., Formulation and evaluation of a salted-out isoniazid-loaded nanosystem, AAPS PharmSciTech 9 (1) (2008) 174–181.
[12] S. Gunalan, R. Sivaraj, V. Rajendran, Green synthesized ZnO nanoparticles against bacterial and fungal pathogens, Prog. Nat. Sci.: Mater. Int. 22 (6) (2012) 693–700.
[13] R. Najafi-taher, et al., Promising antibacterial effects of silver nanoparticle-loaded tea tree oil nanoemulsion: a synergistic combination against resistance threat, AAPS PharmSciTech 19 (3) (2018) 1133–1140.
[14] K. Biswas, et al., Biological activities and medicinal properties of neem (Azadirachta indica), Curr. Sci. Bangalore 82 (11) (2002) 1336–1345.
[15] A. Sirelkhatim, et al., Review on zinc oxide nanoparticles: antibacterial activity and toxicity mechanism, Nano-Micro Lett. 7 (3) (2015) 219–242.
[16] M. Čepin, et al., Morphological impact of zinc oxide particles on the antibacterial activity and human epithelia toxicity, Mater. Sci. Eng. C 52 (2015) 204–211.
[17] M. Divya, et al., Synthesis of zinc oxide nanoparticle from Hibiscus rosa-sinensis leaf extract and investigation of its antimicrobial activity, Res. J. Pharm. Biol. Chem 4 (2) (2013) 1137–1142.
[18] H. Meruvu, et al., Synthesis and characterization of zinc oxide nanoparticles and its antimicrobial activity against Bacillus subtilis and Escherichia coli, J. Rasayan Chem 4 (1) (2011) 217–222.
[19] M.F. Sohail, et al., Folate grafted thiolated chitosan enveloped nanoliposomes with enhanced oral bioavailability and anticancer activity of docetaxel, J. Mater. Chem. B 4 (37) (2016) 6240–6248.
[20] H.S. Sarwar, et al., Design of mannosylated oral amphotericin B nanoformulation: efficacy and safety in visceral leishmaniasis, Artificial cells, nanomedicine, and biotechnology 46 (sup1) (2018) 521–531.
[21] H. Derikvandi, A. Nezamzadeh-Ejhieh, Increased photocatalytic activity of NiO and ZnO in photodegradation of a model drug aqueous solution: effect of coupling, supporting, particles size and calcination temperature, J. Hazard Mater. 321 (2017) 629–638.
[22] Y. Lv, et al., Physico-chemical properties, phytochemicals and DPPH radical scavenging activity of supercritical fluid extruded lentils, Lebensm. Wiss. Technol. 89 (2018) 315–321.
[23] A.A. Yusuf, et al., Free radical scavenging, antimicrobial activities and effect of sub-acute exposure to Nigerian Xylopia Aethiopica seed extract on liver and kidney functional indices of albino rat, Iranian J. Toxicol. 12 (3) (2018) 51–58.
[24] M.F. Sohail, et al., Cell to rodent: toxicological profiling of folate grafted thiomer enveloped nanoliposomes, Toxicol. Res. 6 (6) (2017) 814–821.
[25] A. Verma, M.S. Mehata, Controllable synthesis of silver nanoparticles using Neem leaves and their antimicrobial activity, J. Radiat. Res. Appl. Sci. 9 (1) (2016) 109–115.
[26] M. Sundrarajan, S. Ambika, K. Bharathi, Plant-extract mediated synthesis of ZnO nanoparticles using Pongamia pinnata and their activity against pathogenic bacteria, Adv. Powder Technol. 26 (5) (2015) 1294–1299.
[27] J.W. Olesik, P.J. Gray, Considerations for measurement of individual nanoparticles or microparticles by ICP-MS: determination of the number of particles and the analyte mass in each particle, J. Anal. At. Spectrom. 27 (7) (2012) 1143–1155.
[28] H. Sies, Oxidative stress: a concept in redox biology and medicine, Redox biology 4 (2015) 180–183.
[29] I.F. Benzie, J.J. Strain, The ferric reducing ability of plasma (FRAP) as a measure of "antioxidant power": the FRAP assay, Anal. Biochem. 239 (1) (1996) 70–76.
[30] F. Aqil, I. Ahmad, Z. Mehmood, Antioxidant and free radical scavenging properties of twelve traditionally used Indian medicinal plants, Turk. J. Biol. 30 (3) (2006) 177–183.
[31] H. Tohma, et al., Antioxidant activity and phenolic compounds of ginger (Zingiber officinale Rosc.) determined by HPLC-MS/MS, J. Food Meas. Charact. 11 (2) (2017) 556–566.
[32] S.H. Nile, A.S. Nile, Y.-S. Keum, Total phenolics, antioxidant, antitumor, and enzyme inhibitory activity of Indian medicinal and aromatic plants extracted with different extraction methods, 3 Biotech 7 (1) (2017) 76.
[33] S. Gonçalves, et al., Phenolic profile, antioxidant activity and enzyme inhibitory activities of extracts from aromatic plants used in Mediterranean diet, J. Food Sci. Technol. 54 (1) (2017) 219–227.
[34] C.A. Torres, et al., In vitro antioxidant, antilipoxygenase and antimicrobial activities of extracts from seven climbing plants belonging to the Bignoniaceae, J. Inter. Med. 16 (4) (2018) 255–262.
[35] K.R. Raghupathi, R.T. Koodali, A.C. Manna, Size-dependent bacterial growth inhibition and mechanism of antibacterial activity of zinc oxide nanoparticles, Langmuir 27 (7) (2011) 4020–4028.
[36] P.K. Mishra, et al., Zinc oxide nanoparticles: a promising nanomaterial for biomedical applications, Drug Discov. Today 22 (12) (2017) 1825–1834.
[37] A. Aditya, et al., Zinc oxide nanoparticles dispersed in ionic liquids show high antimicrobial efficacy to skin-specific bacteria, ACS Appl. Mater. Interfaces 10 (18) (2018) 15401–15411.
[38] K. Gold, et al., Antimicrobial activity of metal and metal-oxide based nanoparticles, Adv. Therapeut. 1 (3) (2018) 1700033.
[39] K.M. Reddy, et al., Selective toxicity of zinc oxide nanoparticles to prokaryotic and eukaryotic systems, Appl. Phys. Lett. 90 (21) (2007) 213902.
[40] U. Saleem, et al., Is folklore use of Euphorbia helioscopia devoid of toxic effects? Drug Chem. Toxicol. 39 (2) (2016) 233–237.
[41] G.-L. Shen, J.D. Ng, X.-P. Ma, Etiology, diagnosis, management and outcomes of epiphora referrals to an oculoplastic practice, Int. J. Ophthalmol. 9 (12) (2016) 1751.
[42] K. Rajkumar, N. Kanipandian, R. Thirumurugan, Toxicity assessment on haemotology, biochemical and histopathological alterations of silver nanoparticles-exposed freshwater fish Labeo rohita, Appl. Nanosci. 6 (1) (2016) 19–29.

[43] C. Lasagna-Reeves, et al., Bioaccumulation and toxicity of gold nanoparticles after repeated administration in mice, Biochem. Biophys. Res. Commun. 393 (4) (2010) 649–655.
[44] A. Tiwari, et al., An amperometric urea biosensor based on covalently immobilized urease on an electrode made of hyperbranched polyester functionalized gold nanoparticles, Talanta 78 (4–5) (2009) 1401–1407.
[45] W. Song, et al., Role of the dissolved zinc ion and reactive oxygen species in cytotoxicity of ZnO nanoparticles, Toxicol. Lett. 199 (3) (2010) 389–397.
[46] T. Xia, et al., Comparison of the mechanism of toxicity of zinc oxide and cerium oxide nanoparticles based on dissolution and oxidative stress properties, ACS Nano 2 (10) (2008) 2121–2134.
[47] J. Santhoshkumar, S.V. Kumar, S. Rajeshkumar, Synthesis of zinc oxide nanoparticles using plant leaf extract against urinary tract infection pathogen, Res. Eff. Technol. 3 (4) (2017) 459–465.